Natural Resources Canada | Ressources naturelles Canada

GEOLOGICAL SURVEY OF CANADA
OPEN FILE 7931

Preliminary results of a Magnetotelluric survey in the Chantrey-Thelon area; GEM-2 Thelon tectonic zone project

B. Roberts, J.A. Craven, R.G. Berman, and E. Roots

2015

Canada

GEOLOGICAL SURVEY OF CANADA
OPEN FILE 7931

Preliminary results of a Magnetotelluric survey in the Chantrey-Thelon area; GEM-2 Thelon tectonic zone project

B. Roberts[1], J.A. Craven[1], R.G. Berman[1], and E. Roots[2]

[1] Geological Survey of Canada, 615 Booth Street, Ottawa, Ontario
[2] Simon Fraser University, 8888 University Dr, Burnaby, British Columbia

2015

doi:10.4095/297426

This publication is available for free download through GEOSCAN (http://geoscan.nrcan.gc.ca/).

Recommended citation

Roberts, B., Craven, J.A., Berman, R.G., and Roots, E., 2015. Preliminary results of a Magnetotelluric survey in the Chantrey-Thelon area; GEM-2 Thelon tectonic zone project; Geological Survey of Canada, Open File 7931, 29 p. doi:10.4095/297426

Publications in this series have not been edited; they are released as submitted by the author.

Table of Contents

Table of Figures 1
Introduction 2
Geological Background 3
MT Acquisition 5
Data Processing and Editing 7
Data Analysis 8
2D Modelling 9
3D Modelling 10
Discussion 15
Conclusions 17
Acknowledgements 18
References 18
Table 2. 20
Appendix A. 21
Appendix B. 25

Table of Figures

Figure 1: Aeromagnetic map of project area, showing MT site locations (numbered) and bedrock mapping observation points (white x's), with inset showing location in Canada. 2
Figure 2: Bedrock compilation geology map with MT sites and section lines for slices through the 3D model that are presented in the report (see Figure 8). 4
Figure 3: Photos depicting typical conditions for a MT site during the TTZ project; A. a site being laid out in a sandy flat lying area, B. a site being left to record overnight with the MTU recorder and battery loosely wrapped in a tarp for protection. 5
Figure 4: Response curves (resistivity and phase) for processed and edited data from site ttz208 displayed for three different azimuths (0, -19, and -47 degrees). 7
Figure 5: Aeromagnetic map of project area, showing MT site locations and results from the decomposition analysis that provides an estimate of electrical strike direction at each site. The average strike direction for all sites in the 100 Hz to 10 Hz band is -19 degrees (black arrows show result for individual site) and for longer periods the average is -47 degrees (red arrows). ...9
Figure 6: Hybrid 2D conductivity model along the southern profile showing the corresponding strip through the aeromagnetic map and MT sites along the top. 10
Figure 7: A 2D plan view of the 3D grid used for the MT inversion and the MT site locations. .11
Figure 8: Two sections through the 3D conductivity model (A. section 1, B. section 2; see Figure 2 for section locations) with bars at the top which show the corresponding geology (from Figure 2) and MT sites. The geological bars are aligned such that the section line goes directly along the top of the MT model and some geology in the northward direction is included. 12
Figure 9: Six depth slices through the 3D conductivity model. 13
Figure 10: A comparison of the 2D model and section 1 of the 3D model along the southern profile of MT sites. Rough outlines of the conductive zones observed in the 3D model have been overlain on the 2D model for comparison. A: The hybrid 2D model from Figure 6. B: Section 1 from the 3D model with highly conductive zones outlined. C: 2D model using azimuth of -47 degrees. D: Section 1 from 3D model with broadly conductive zones outlined. 14

Introduction

The Thelon tectonic zone (TTZ) project is part of the second phase of the Geo-mapping for Energy and Minerals program (GEM-2) in which a multi-disciplinary approach is being used to better understand the geological history and crustal architecture in this zone. The TTZ occurs at the western margin of the Rae craton in Nunavut, separating the Slave from the Churchill (Rae) structural provinces, and represents a complex suture zone formed during both subduction and continental collision (Hoffman, 1988). Parts of the TTZ underwent systematic geological mapping in the 1980's following reconnaissance work in the early 1960's, however, a more detailed geological/geophysical understanding and integrated database is required to attract mineral exploration to this frontier area (Berman, et al., 2015). The project includes bedrock mapping, surficial sampling, geochemical surveys, and a magnetotelluric (MT) survey. The primary goal of the MT component of the project is to help define the crustal architecture of the TTZ and determine how the Slave and Rae cratons interacted in this area.

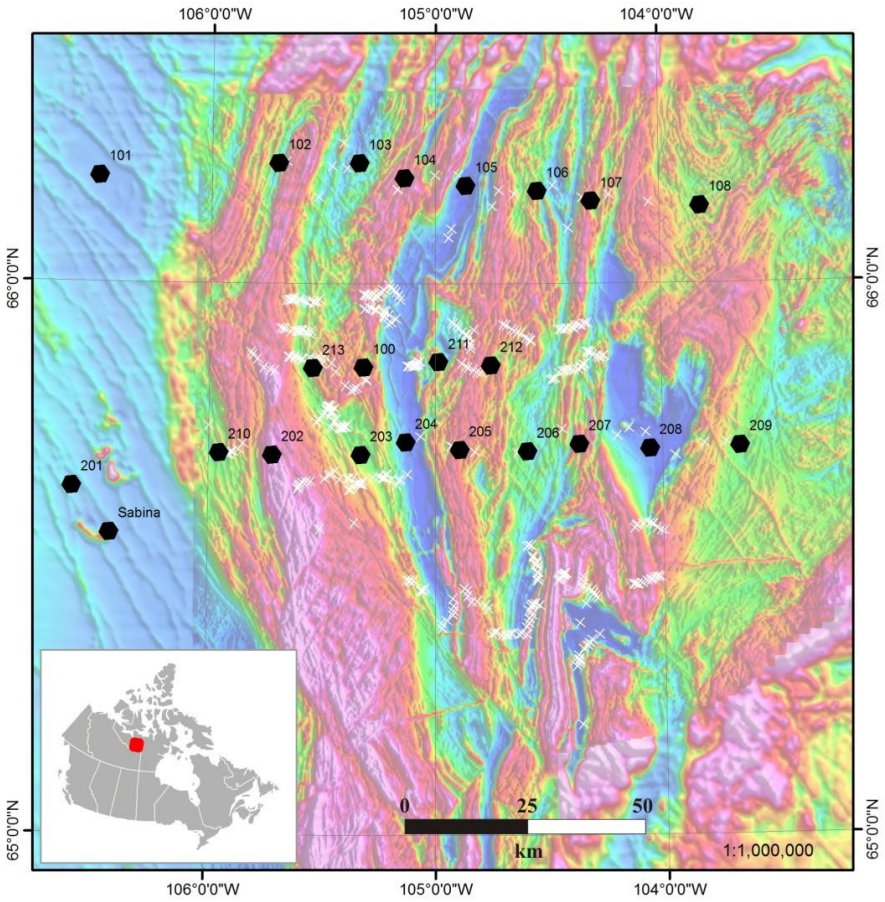

Figure 1: Aeromagnetic map of project area, showing MT site locations (numbered) and bedrock mapping observation points (white x's), with inset showing location in Canada.

The MT method provides information on the electrical conductivity of the subsurface through the measurement of natural time-varying electric and magnetic fields in orthogonal directions at the surface. Due to the dependence of the depth of investigation of the fields on their frequency, an estimate of conductivity variation with depth can be attained. A total of 22 broadband MT sites were collected, primarily along two approximately East-West transects, during the summer of 2014 (Fig. 1). The data have been processed and edited to produce response functions at all sites, a strike analysis has been performed, and modelling has been initiated. Presently, we have a 2D model along the southern transect and a 3D model utilizing all but one of the sites, and these can be compared to aeromagnetic and geological observations. Currently, we are investigating the reliability of significant features in the MT model and hence features presented here must be considered preliminary.

Geological Background

The MT survey spans the boundary between the eastern Slave craton and the Thelon tectonic zone (TTZ) on the western flank of the Rae craton (Fig. 2). The TTZ comprises a series of pronounced, N- to NNE-striking magnetic anomalies that extend ~500 km from the MacDonald fault to the Queen Maud Gulf. The TTZ has been postulated to represent a continental arc built on the western flank of the Rae craton and subsequently intensely deformed during collision with, and indentation by the Slave craton (Hoffman, 1988). Alternative models propose that the TTZ formed in an intracontinental setting either after crustal thinning (Thompson et al., 1989) or within an interior mountain belt far removed from an active plate boundary (Chacko et al., 2000; Schultz et al., 2007).

The eastern Slave craton is dominated by metasedimentary and metavolcanic rocks of the Yellowknife Supergroup intruded by 2.61 – 2.58 Ga granitoids (Frith, 1982; Thompson et al., 1986). Metamorphic grade increased eastward from lower- to upper-amphibolite facies during both Neoarchean and Paleoproterozoic (Thelon orogeny) events. This gradient culminates northeast of the Bathurst fault (Fig. 2), where the proportion of supracrustal rocks decreases as deeper crustal levels expose migmatitic granitoid gneisses interspersed with thin metavolcanic belts (Thompson et al., 1986).

The western Rae craton consists largely of Mesoarchean upper amphibolite to granulite facies granitoid rocks of the Queen Maud block (QMb; Figure 2). A thin belt of ca. 2.0 Ga metagranitoid rocks (eastern plutonic belt; Fig. 2; Davis et al., 2013) separates a Mesoarchean crustal domain (Duggan Lake domain; Fig. 2) that bears strong similarities with the Queen Maud block (Berman et al., 2015b). In several places, these plutonic rocks are associated with magnetite-bearing diatexites (Berman et al., 2015a, b) which may be the source rocks of a significant Au anomaly in this region (McCurdy et al., 2013).

The extent of Rae and Slave craton within the TTZ has not been well established. The pronounced, >100 km long magnetic low on the west side of the Mesoarchean domain (Md, Fig. 2) largely comprises variably strained garnet leucogranite that potentially formed from melting of Rae margin sediments (Berman et al., 2015b). This would put the edge of the Rae craton (S1, Figure 2) ~ 60 km east of the boundary based on the distribution of Yellowknife Group supracrustal rocks (S2, Fig. 2; Thompson,

1992) and ~ 40 km east of a Slave-Rae suture (Culshaw, 1991; Hoffman and Hall, 1993) corresponding to the western limit of recognized Paleoproterozoic plutonic rocks (S3; Thompson et al., 1986; Fig. 2).

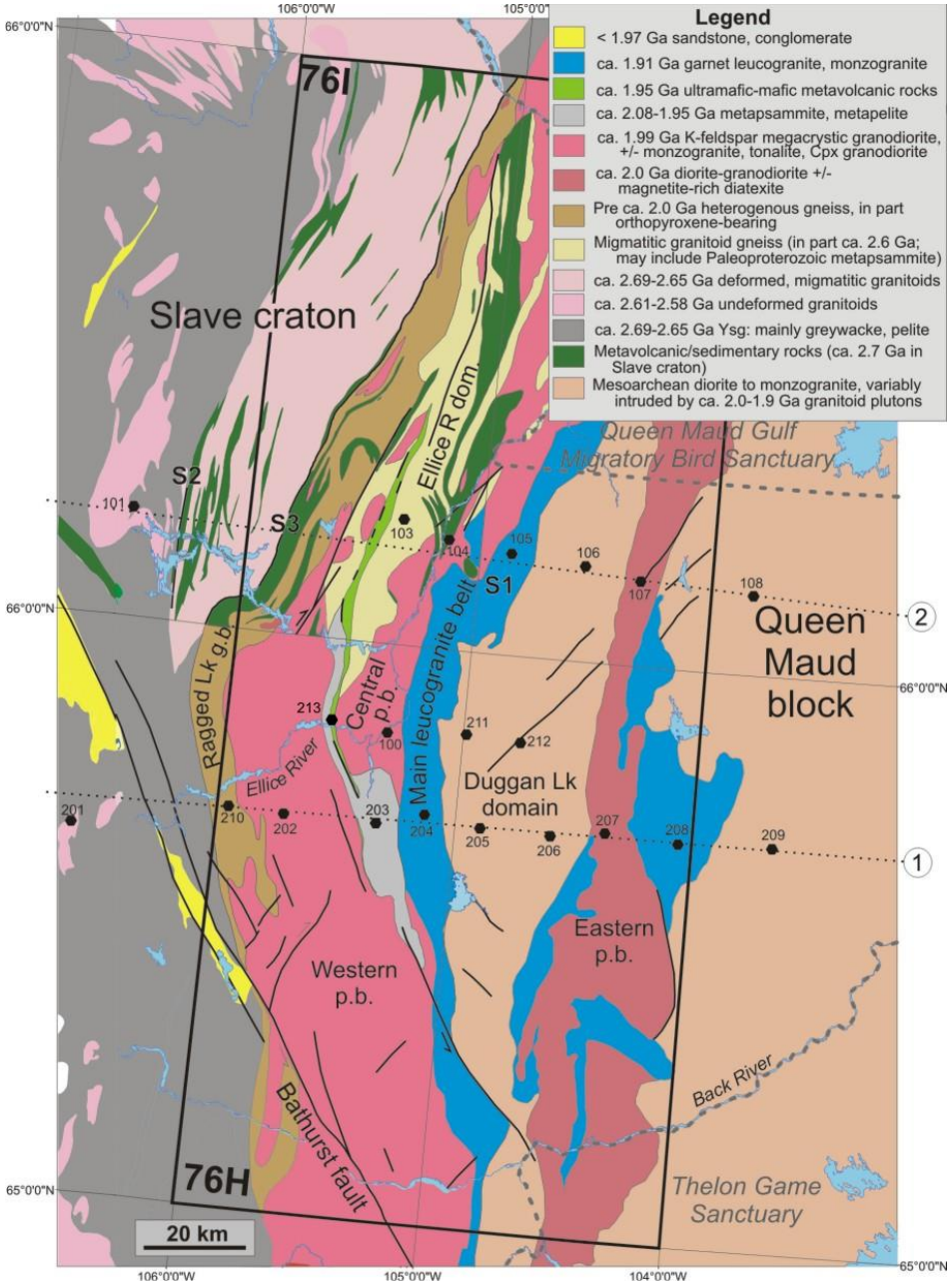

Figure 2: Bedrock compilation geology map with MT sites and section lines for slices through the 3D model that are presented in the report (see Figure 8).

The upper amphibolite to granulite facies region between alternate suture locations S1 and S3 is marked by a pair of prominent magnetic highs consisting of ca. 1.99 Ga metaplutonic rocks (western and central plutonic belts; Fig. 1) that are intrusive into high-grade gneisses as old as 2.03 Ga (Davis et al., 2014). The pedigree of the crustal domain between these two belts is presently unknown, but a ca. 2.59 Ga age of monzogranite gneiss (Davis et al., 2014) suggests affinity with the Slave craton. This crustal domain

(Ellice River domain; Fig. 2) hosts a 1.95 Ga ultramafic to mafic metavolcanic belt (Davis, unpublished data; Berman et al., 2015b) which is spatially associated with pronounced geochemical anomalies (e.g. Ag, Pb, Cu, Zn, Ni, U; McCurdy et al., 2013), and interstratified with well foliated Paleoproterozoic psammitic rocks at anomalously low metamorphic grade (lower amphibolite facies) compared to surrounding rocks.

MT Acquisition

The MT fieldwork was performed from June 25 to July 13, 2014 and was based out of a field camp located on a sandy plateau overlooking the Ellice River, approximately 100 km SE of Bathurst Inlet, Nunavut (Fig. 1). The camp was assembled from June 23 to 25 and helicopter deployments (Bell 206L4) of the MT equipment began June 26. The last deployment was July 12 and full camp demobilization was completed by July 16. Broadband (BBMT) data were acquired at 22 site locations along two approximately 140 km long, East-West corridors that run across the geological strike of the TTZ from the Slave craton into the Rae, with some in-fill stations at the same latitude as the base camp. Nominal site spacing along the lines was 15-20 km. The data were collected using GSC and POLARIS MTU-5a recording instruments. The magnetic sensors for this survey were chosen with a view to their relative low weight and low battery power draw due to the inherent remoteness of the survey area and project focus on crustal architecture rather than mantle information. As such, MTC80 (horizontal components) and AMTC (vertical component) magnetic coils (Table 1) were selected for this survey. The AMTC coils are the shortest of the various coils manufactured by Phoenix and therefore easier to install in the earth to measure the vertical component of the magnetic field. The electric fields were recorded in two horizontal, perpendicular directions using lead-lead-chloride porous pot electrodes. The majority of sites were installed using three magnetic sensors (two horizontal and one vertical). However, site conditions and equipment issues caused several sites to be recorded with only the horizontal components and one site to be recorded E-only (i.e. no magnetic coils) (Table 2). This is not a problem as the magnetic field is nearly uniform spatially and synchronization of recording means magnetic information from a nearby site can be utilized. The minimum recording time was overnight (at least 15

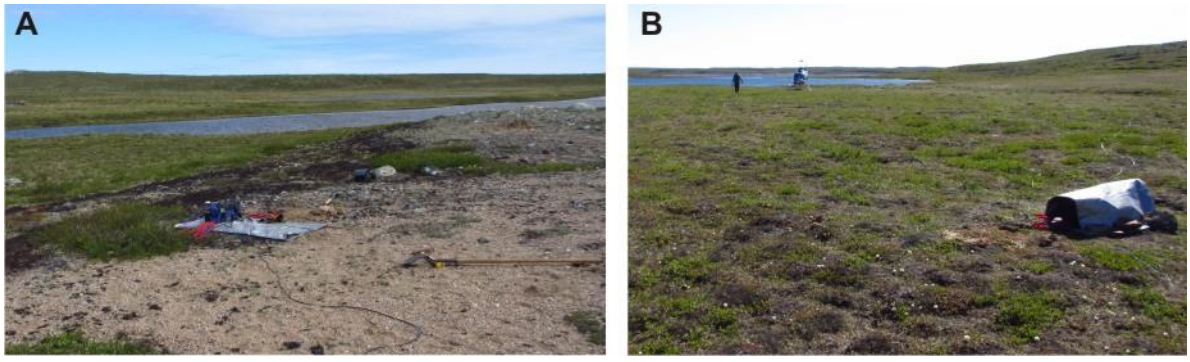

Figure 3: Photos depicting typical conditions for a MT site during the TTZ project; A. a site being laid out in a sandy flat lying area, B. a site being left to record overnight with the MTU recorder and battery loosely wrapped in a tarp for protection.

hours) and some sites were either re-sounded for additional nights, or installed with extra batteries and left to record for multiple nights. Maximum recording time was 4 nights at site ttz201 (Table 2). The terrain in the project region is undulating and mostly covered with glacial till, with sporadic outcrop. MT sites were located in flat low lying areas where mud boils could be used for burying electrodes as much as possible, and some dry till (sand, soil mix) was available for installing the magnetic sensors (Fig. 3). All electrode lines were pinned to the ground with rocks or sand to minimize wind noise and tarps were used to protect the MTU recorder from rain (Fig. 3).

We experienced numerous difficulties with the recordings at many sites, especially in the first week of the survey. On a number of occasions, when a site was to be retrieved, the MTU was still powered on, but in an error state not able to communicate with the computer. At these stations, the successful data recording window would typically be short (several hours at most) and the data unusable. There were some cases where 7-10 hours of data had recorded and could be used. Possible causes that were considered included; overheating due to long days with higher than normal temperatures, problems with one or more magnetic sensors, bad Compact Flash (CF) cards, and faulty MTUs. Equipment was rotated in and out of sites to help narrow down potential hardware problems and the recorders were shielded from the sun as much as possible to control temperatures, but the problems persisted intermittently. Eventually it was determined that a set of new 2 GB CF cards were causing these sporadic MTU failures and a reliable set of older, smaller capacity cards were assembled to finish the survey. This problem affected the production as far as decreasing the number of sites that could be recorded, but the minimum planned survey was exceeded and only one site (ttz102) never produced a usable time series. Site ttz100 was situated near the camp (approximately 200m from infrastructure) and there was a high amount of electrical noise from the generators and internet setup. However, some good recordings were made early before the internet hardware was installed, and the site was also used to troubleshoot suspected equipment issues.

Table 1. GEM-2 TTZ MT survey equipment

Equipment	**Quantity**	**Serial Numbers**
Phoenix Geophysics MTU-5A recorders	4	1562, 1561, 1493, 1496
MTC80C Phoenix magnetic coils	2	8052, 8053
MTC80H (high gain) Phoenix magnetic coils	6	7320, 7513, 7322, 7319, 8051, 7509
AMTC Phoenix magnetic coils	3	1145, 1328, 1147

Data Processing and Editing

Digital data for the three magnetic field sensors and two electrical components collected at a site during the MT survey were saved as time series, but for analysis and modelling the data were converted to frequency dependent transfer functions. This data processing step is referred has the effect of greatly decreasing the amount of data. After using a Fourier transform to convert the data from the time domain to the frequency domain, the data reduction is achieved by weighted stacking of the data falling in particular spectral bands. Data processing was performed in the field using a Windows based laptop and the SSMT2000 program from Phoenix Geophysics. SSMT2000 performs robust remote reference processing (method 6 of Jones, et al., 1989) of the Fourier coefficients producing power spectral estimates, termed crosspowers. Stacked estimates at 20 regular recording intervals for each site were viewed and edited at each frequency using the Phoenix program MT Edit. During this step, the data quality was verified and poor data points eliminated. At this point the recording parameters were assessed and a decision made as to whether or not more data were required at a specific site. This was particularly important early in the survey.

Spectral information is not useful for the interpretation of subsurface structure, however, the transfer functions between the two components of each of the horizontal electric field and magnetic field power spectrums define four impedance terms. Each of the four MT impedance terms has a real and imaginary part that can be expressed as an amplitude called an apparent resistivity, a spatial average of the true resistivity in the subsurface proximal to the site, and an impedance phase related to the change of the apparent resistivity with frequency. Figure 4 shows the processed and edited results for site ttz208. The overall data quality was very good in the period range .01 – 100 s, but decreased for periods above 100 s as expected for the sensor coils selected for this survey. Plots of all sites recorded are shown in Appendix A.

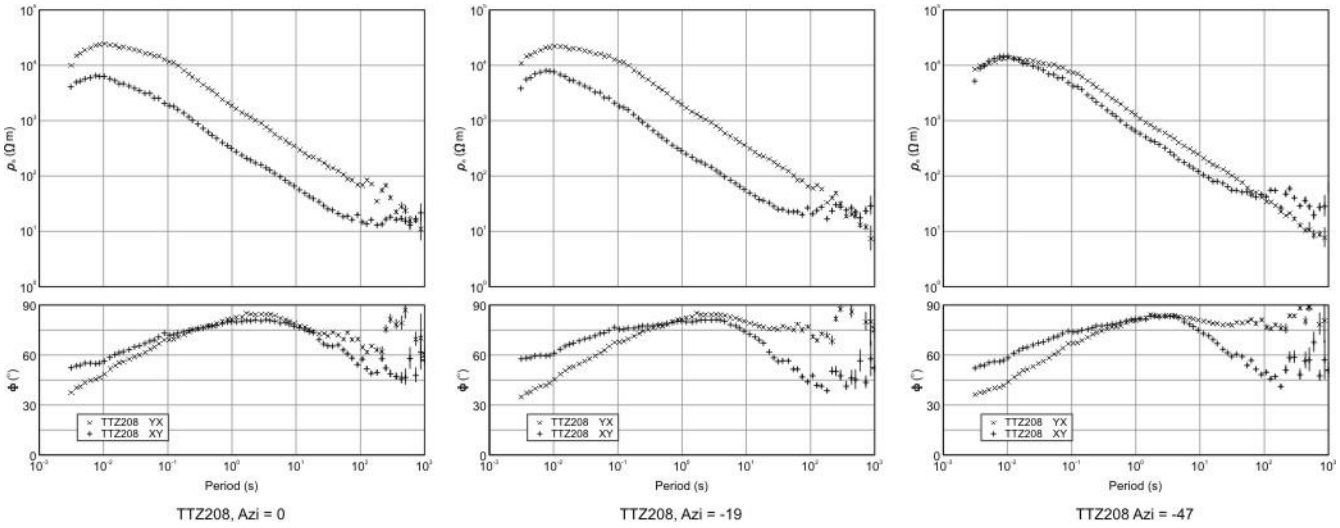

Figure 4: Response curves (resistivity and phase) for processed and edited data from site ttz208 displayed for three different azimuths (0, -19, and -47 degrees).

Data Analysis

MT data can be analysed using a variety of methods to unravel the subsurface structure. It is important to use a method suited to the regional structure in the area. For example, layered earth (i.e. 1-D) analysis methods may be used in the interior of sedimentary basins where there is a limited azimuthal dependency on resistivity. Areas, such as the Cordilleran orogeny, for example, with a long, relatively uniform regional strike should be approached using 2-D analysis methods. In 2-D model studies one spatial direction (into and out of the plane of a profile, termed either the geo-electric strike direction or simply the strike direction) is considered to be invariant in terms of resistivity or at least to have so little variation so to be of no effect on the data. In more complicated areas, where there is no such invariant direction and structure varies strongly in all three directions, only fully 3-D analysis methods can be utilized. In general, the more dimensions modelled, the more limitations there are on the number of sites and data that can be modelled, in addition to an increasing limit on the effective number and size of the cells in the model. As such, it is fairly common to use 2-D inversion methods to derive the structure wherever permissible as they offer a balance of model resolution and accuracy whilst also affording the advantage of being able to work with a large amount of data. However, before a 2-D inversion is contemplated a procedure should be used to determine the applicability of 2-D methods to the data set in hand; or at least identify frequency bands or sites which are amenable to 2-D analysis. The method should also provide an estimate of the strike direction for a data set. Figure 4 demonstrates the effect of changing azimuth on the resistivity and phase curves for a sample MT site (ttz208), indicating an inappropriate choice will lead to erroneous data and ensuing models.

The method we have utilized (McNeice and Jones, 2001) is based on the Groom-Bailey (1989) decomposition analysis which evaluates the separation of the observed MT tensor, on a site by site and frequency by frequency basis, into a regional strike direction and tensors appropriate for a 2-D regional structure and the effect of small-scale near surface scattering bodies. The McNeice and Jones method works with bands of frequencies and across a set of sites to stabilize and speed up the analysis procedure. The technique calculates an nRMS (root-mean-square misfit normalized by error) misfit between the product of the decomposed set of tensors and the observed tensor as a guide to the appropriateness of a 2-D approximation in the area. One weakness of this technique is the estimate of the strike direction suffers from a 90 degree ambiguity; as such other information has to be utilized to constrain the strike. For this survey we deployed vertical field sensors as the ratio of horizontal to vertical field components can possess characteristic spatial patterns which can be used to identify the edges of 2-D conductors and thereby remove the ambiguity in the strike direction. This technique has limitations as the vertical field is weaker in strength and more difficult to sense than the horizontal components. Further exacerbating the issue is the fact we used only high frequency sensors (induction coils) to measure the vertical components. The use of these coils ultimately limits this technique to primarily the 100 Hz to 10 Hz band for the most robust estimate of the magnetic field component ratio.

The results in Figure 5 are based on individual site McNeice-Jones analysis for multiple bands. The arrows point along the estimated geo-electric strike direction at each site for each band; and estimates

associated with higher nRMS in the misfit exercise are shown with shorter arrow lengths. They generally show geo-electric strike directions parallel to aeromagnetic fabric at the shortest period bands corresponding to shallower depths. At longer periods the directions predominantly rotate counter clockwise. To characterize the shallow, short period, strike directions and the deeper, long period strike directions two further analyses were run on data for all sites. The average strike directions for the 100 Hz to 10 Hz band was -19 degrees from T.N., and the longer period data has an average direction of -47 degrees T.N. As mentioned before there is a 90 degree ambiguity in the decomposition analysis which has to be addressed with other data. The alignment with the aeromagnetic fabric is justification itself for our choice of -19 rather than +71; however the ratio of the real parts of the magnetic field components are shown as arrows in Figure 5 plotted with the convention to point towards conductors. As such they confirm the analysis based on the aeromagnetic fabric. The choice at longer period (i.e. -47 or +43) is more problematic, but the strikes appear to rotate to -47 from -19 in the band by band analysis and the final direction appears to align with the direction of a predominant major fault in the area (the Bathurst fault; Fig. 2).

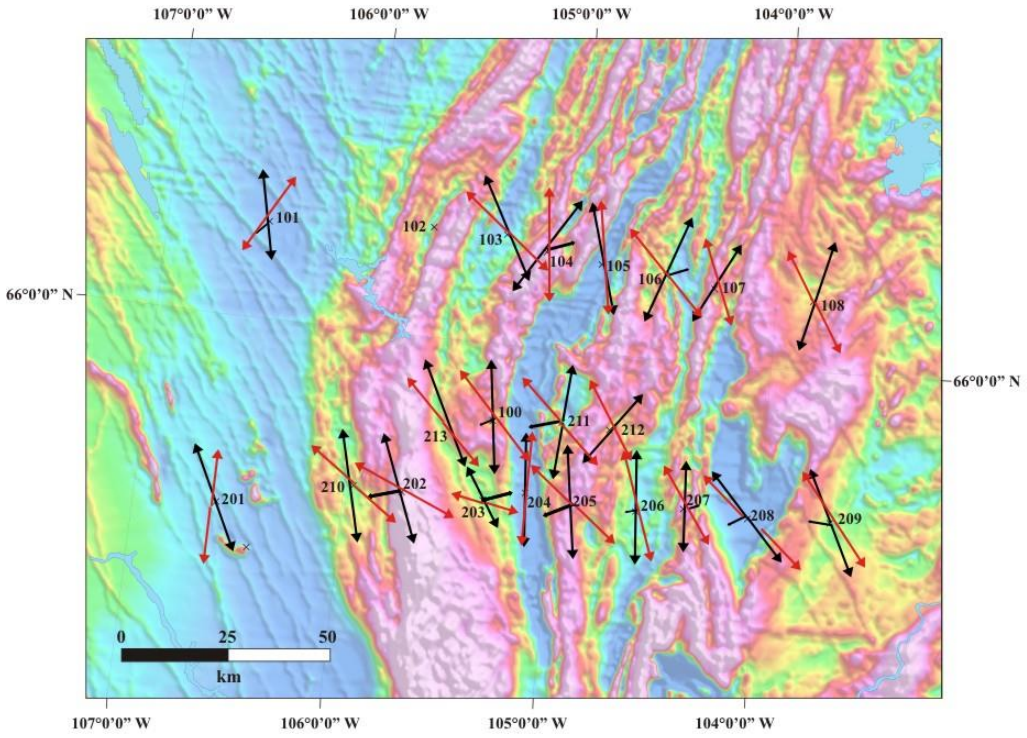

Figure 5: Aeromagnetic map of project area, showing MT site locations and results from the decomposition analysis that provides an estimate of electrical strike direction at each site. The average strike direction for all sites in the 100 Hz to 10 Hz band is -19 degrees (black arrows show result for individual site) and for longer periods the average is -47 degrees (red arrows).

2D Modelling

Two dimensional modelling was completed along the Southern transect (sites 201 – 210) using the WinGLink™ implementation of the Rodi and Mackie (2001) inversion scheme. Initially, the regional 2-D tensor estimates from the McNeice-Jones algorithm were used in the band 100Hz to 100s for an

azimuth of -19 degrees. The data were inverted for 100 iterations from a starting half-space model of 3000 ohm m with large errors on the resistivity set to 20%, phase TE error set to 5 degrees, and phase TM error set to 2 degrees to reflect the fact that TM phases are generally least affected by off-line structure not modelled properly in 2-D algorithms. This process was repeated for a broad range of inversion trade-off parameters (tau) to define a curve of model misfit vs model smoothness. A value of tau=3 was chosen for further inversions as the best compromise between model structure and misfit. The data were then inverted for 10 iterations to set the static shift parameters and then inverted for a further 100 iterations with static shift fixed arriving at a final nRMS of 2.33. This process was repeated for a strike direction of -47. An attempt was made to utilize the model at -19 as a starting model for inversion of the data -47; however all attempts to fit the data using a variety of constraints on the model parameters failed. The result of the modelling exercise is two models with structure that is more reliable at certain, but unspecific, depth ranges. The model using an azimuth of -19 is reliable at shallow depth whereas the model done at -47 is more reliable at greater depths (i.e. longer periods).

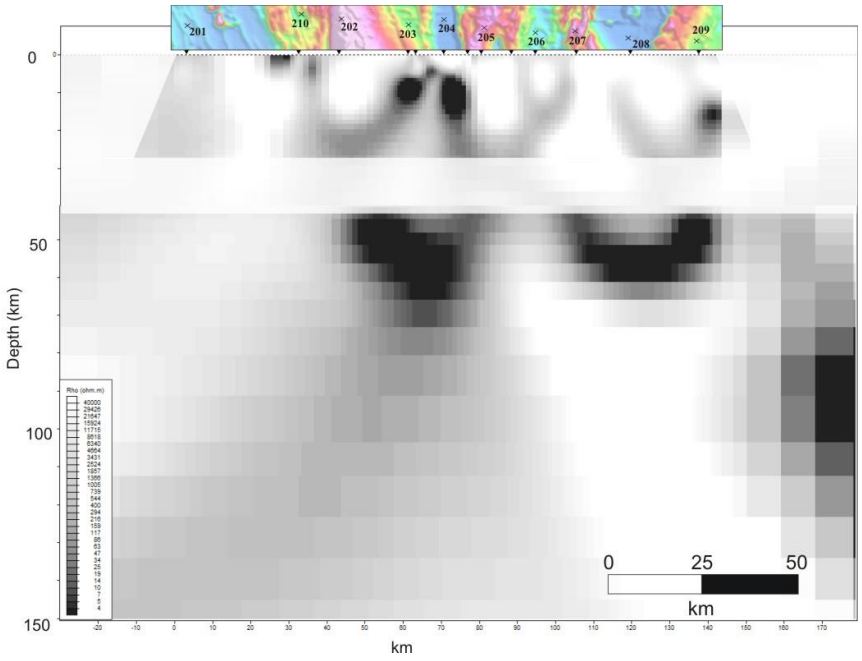

Figure 6: Hybrid 2D conductivity model along the southern profile showing the corresponding strip through the aeromagnetic map and MT sites along the top.

Having two models for a single line is unsatisfactory for interpretational purposes. Hence a hybrid model (Fig. 6) was constructed using crustal elements of the model at -19 degrees and deeper elements from the model obtained at -47 degrees. In general, it was found during this exercise that the two models do in fact have similar structure at mid-crustal depths (i.e. no large tear in model structure exists where the two models meet), however this area has been de-emphasized as model uncertainties are large and a 3-D model should be viewed as more reliable.

3D Modelling

To invert the data in 3D we utilize a program WSINV3DMT that has been developed based on an Occam inversion method, and which seeks a minimum structure to provide an appropriate fit to the data (Siripunvaraporn et al., 2005). The Occam approach is a stable and robust technique that often converges to the desired misfit in a relatively small number of iterations, typically less than eight

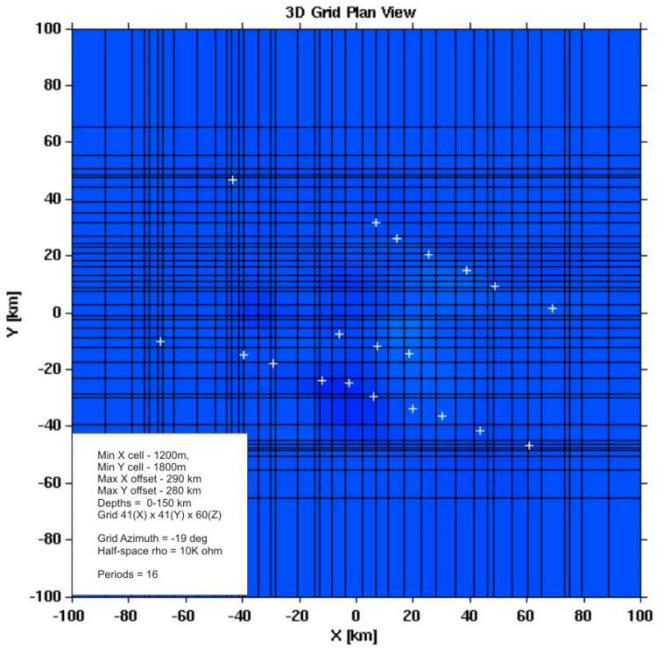

Figure 7: A 2D plan view of the 3D grid used for the MT inversion and the MT site locations.

(Siripunvaraporn and Egbert, 2009). The 3D inversion offers more degrees of freedom than in 2D, enabling 3D effects from outside the profile or cluster of sites to be recovered and the locations of conductors be inserted in their proper position. We implement the program on a multi-node Linux cluster and invert 16 periods between .01 and 100 s, which typically requires 24-36 hours per model. A number of different variations on the starting model were tested, but thus far the 3D grid and parameters as shown in Figure 7 has provided the best match to the observed data for all of the surveyed sites. Orienting the grid and tensor data with geological structure has been identified as advantageous for modelling complex structure when not using the diagonal elements of the impedance tensor during an inversion (Kiyan et al., 2014). We have indeed used the diagonal elements of the impedance tensor, but have down-weighted these elements in the inversion as they have higher associated errors. Based on strike directions attained from the 2D modelling, an azimuth of -19 was utilized for the grid. There is a slight rotation of the 2-D strike directions in the northern line from this value and a deviation in the longer period strike directions at all sites, indicating testing a variety of grid azimuths should be a priority for the next phase of 3D modelling. It was found that superior results could be attained by re-running an inversion using the best model achieved from a previous run as the starting model and slightly modifying the periods used by the program. The inversion results shown here (Figs. 8 and 9) have an overall nRMS error of 1.781. Appendix B shows the match achieved between the 3D model and response curves for the sites that were utilized.

To display the model we show both cross sections and a series of depth slices. The positions of the sections (numbered 1 & 2) shown in Figure 8 are identified in Figure 2 and are more or less perpendicular to the regional strike of the TTZ structures. The sections generally display a more conductive mid/lower crust below interpreted Rae craton, and we observe a rather abrupt change to high crustal resistivities at a location correlating to the surface trace location of S1 shown in Figure 2.

In Figure 8b, corresponding to Section 2, a number of features in the model approach the surface facilitating the correlation of key features in the model with the surface geology. One of the shallowest features in this section is a weakly conductive zone dipping west beneath site 103, located in a migmatitic/psammite domain. This shallow conductor may be related to graphitic material within the migmatites itself or other conductive material in the foliated Paleoproterozoic psammites. To the west of this unit granitic plutonic rocks are resistive. However, west of S2 it appears Slave greywackes and

pelitic material are more conductive, thick and possessive of a westward dip. Features such as these at the perimeter of the model need to be more rigorously tested in follow-up model sensitivity studies. A modest conductor at ~25km depth beneath the deformed granites remains enigmatic. Below the weak conductor at site 103, a stronger conductor at 20km or so depth can be traced upward to the approximate location of the leucrogranitic unit at S1 (Fig. 8b). The resistivity of the feature increases as it

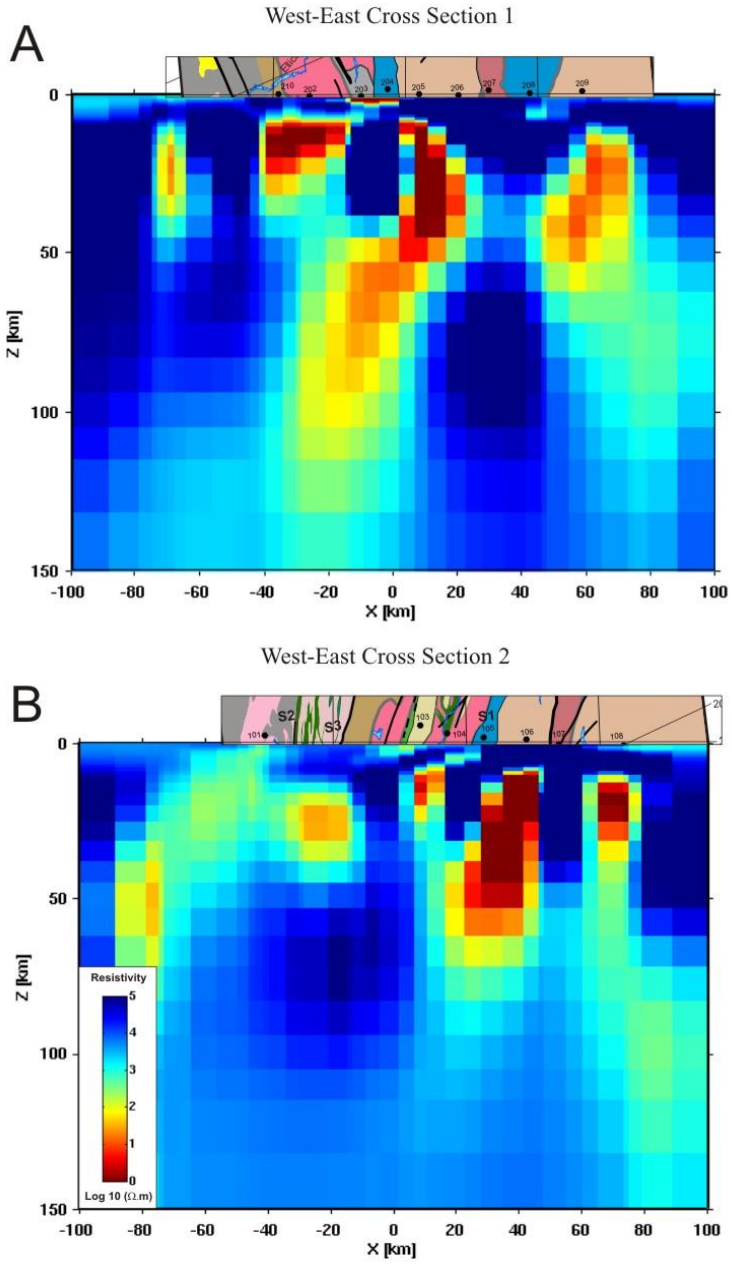

Figure 8: Two sections through the 3D conductivity model (A. section 1, B. section 2; see Figure 2 for section locations) with bars at the top which show the corresponding geology (from Figure 2) and MT sites. The geological bars are aligned such that the section line goes directly along the top of the MT model and some geology in the northward direction is included.

approachs the surface. A crustal-scale, steeply dipping conductor is clearly evident to the east of this conductor and is located at mid to lower crustal depths within rocks associated with the Queen Maud block; but younger leucogranites are also evident near this conductor as well to the south of the transect (Fig. 2). The easternmost conductor also within the Queen Maud block is well off profile and needs further data to refine geometries. We point out that 3D MT methods have recently been shown to reliably image conductive features off-profile (Booker et al., 2014).

Except for the very shallow feature on section 1 (Fig. 8a), below sites 203 and 204, we observe similar features on both sections. There is a weak, shallow conductor below site 103 on section 2, however, the resolving power afforded by the station spacing along the northern transect and measurement bandwidth make it difficult to confidently link it with the shallow feature on section 1.

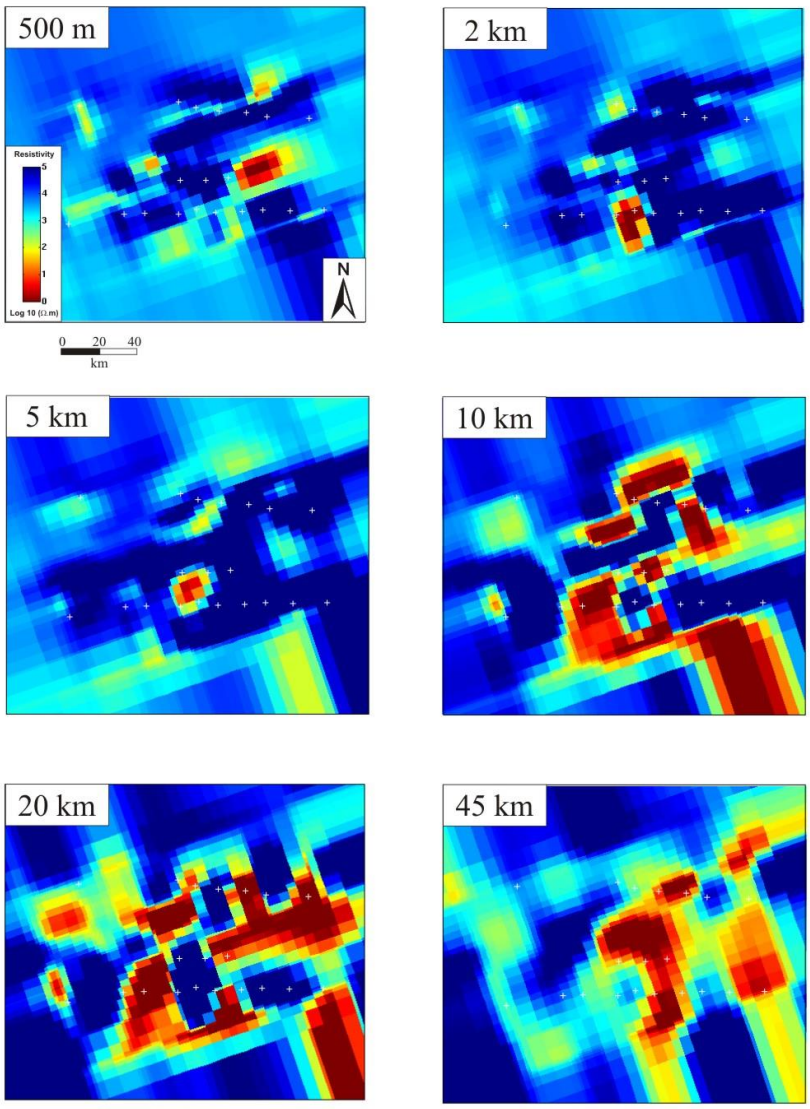

Figure 9: Six depth slices through the 3D conductivity model.

The depth sections through the model (Fig. 9) indicate a predominantly resistive upper crust (0-10 km depth) with a relatively small conductive body near the centre of the project area. At 10 km depth and greater we observe a complicated pattern of higher conductivities that persist until mantle levels. The conductivity patterns observed in the mid/lower crust do not obviously correlate with the belt-like appearance of the TTZ at surface.

When comparing the 2D model with section 1 through the 3D model, (Fig. 10), it is apparent there are discrepancies between the two models. The shallow conductor at X=0 in the 3D model (Fig. 10B) is not evident at all in the hybrid 2D model (Fig. 10A), but in the 2D model attained using an azimuth of -47 degrees we do see a conductor below site 204 that correlates (Fig. 10C). Major features within the crust and mantle appear to be present in both the 2D and 3D models and they generally correlate quite well.

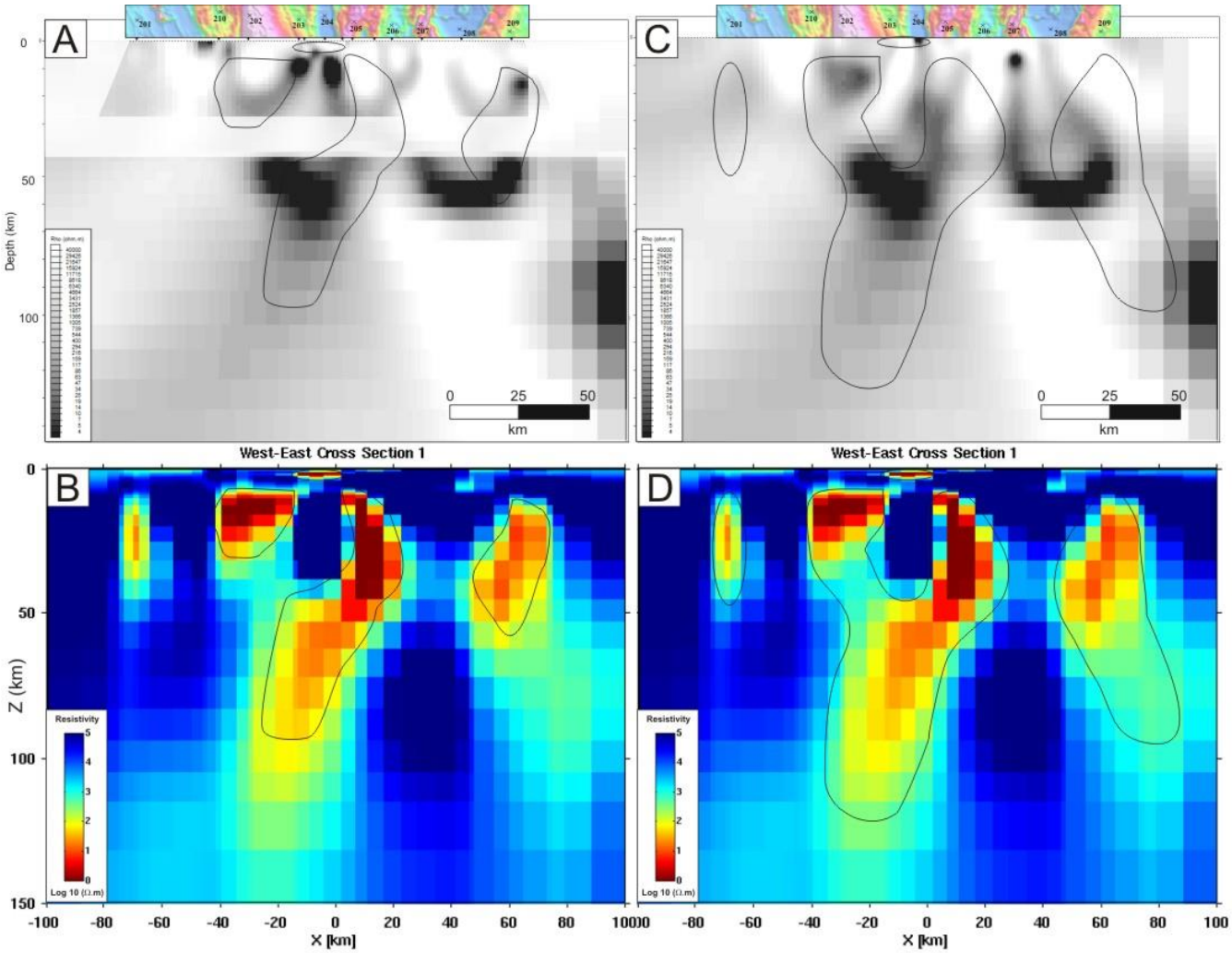

Figure 10: A comparison of the 2D model and section 1 of the 3D model along the southern profile of MT sites. Rough outlines of the conductive zones observed in the 3D model have been overlain on the 2D model for comparison. A: The hybrid 2D model from Figure 6. B: Section 1 from the 3D model with highly conductive zones outlined. C: 2D model using azimuth of -47 degrees. D: Section 1 from 3D model with broadly conductive zones outlined.

Differences are likely due to the fact that although -19 is, on average, the strike direction for the line, it is apparent from Figure 5 that the short period strike directions at the sites in the centre of the line can differ significantly from this average value. Our first thought was the data at these sites, when rotated to –19 degree for 2D modelling, will misrepresent the subsurface structure. The issue with this explanation is that the data rotated to -47 seem to match the 3D model (compare Figs. 10C and D), reiterating the fact that more work on the effect of chosen azimuth is a priority. The disappearance of the shallowest conductor may be related to static shift inversion iterations which will tend to smooth out shallow structures that generate only apparent resistivity and not phase anomalies. Such appears to be much of the case on inspection of the data at sites 203 and 204 in Appendix A where the apparent resistivity curves drop sharply at long periods. The shallowest parts of the conductive zones between X=-40 and 20 on section 1(Fig. 10B) do generally correspond with the two conductive bodies beneath sites 203 and 204 in the hybrid 2D model (Fig. 10A).

Discussion

An understanding of crustal conductivity requires an understanding of the type of mobile charge carriers within a particular rock unit (see Selway, 2014 for a complete review). Mobile charge carriers in a metallic rock unit (such as a sulphide or graphite) are free electrons, whereas the mobile charge carriers in porous rocks are primarily ions within interconnected pore fluids. In addition, at temperatures appropriate for the upper mantle, proton movement either due to crystallographic dislocations or within lattice-held water is thought to be an important charge carrier. The mechanism by which a charge carrier is added to or freed from a rock depends on the particular geological environment. Of relevance to this study of a Paleoproterozoic orogen in which fluids are not be expected at depth, two related mechanisms are thought to be most compelling. While black shales are generally not strongly conductive (Adão et al., 2015), the production of graphite in metasedimentary rocks during metamorphism is a widely accepted mechanism to enhance rock conductivity (e.g., Korja et al., 1996 and Selway, 2014). This mechanism is an important consideration when thick packages of euxinic shales in Paleoproterozoic foredeeps are buried at sutures between major crustal blocks (Boerner, et al., 1996). Secondly, CO_2 rich fluids accompanying granulite facies metamorphism have been proposed as the source of thin conductive graphite films that have been observed coating mineral grains in granulite-facies crustal xenoliths (Frost et al., 1989). These two mechanisms provide a framework to interpret conductive features in MT sections across Proterozoic sutures, and we discuss their applicability to our models below. This interpretation is necessarily preliminary in nature due to two factors. First, a sensitivity analysis is required to test model features such as depths, dips, and along strike continuity of conductors. Second, interpretation of the MT model requires feedback from ongoing bedrock geology studies of rocks exposed at surface. Of particular importance is the need to evaluate what geologic variations along strike may be associated with differences evident in MT sections 1 and 2 (Figs. 8a and 8b).

Our utilization of the framework discussed above, must per force be constrained by relevant geological data observable at the surface. There is no evidence of thick graphite-bearing metasedimentary rocks at the surface but leucogranites, which are abundant in the study area (Fig. 1), are the products of melting of metapelitic material within orogens (Harris and Inger, 1992). However, orogenic models incorporating thickened crust may be insufficient to generate the heat required to melt the pelitic material (Nabelek and Liu, 2004). Nabelek and Liu (2004) suggest thick sequences of sedimentary rocks rich in radioactive material significantly enhance the thermal regime but may still require additional heat from frictional heating along major tectonic boundaries. Thus one model we entertain is that the leucogranites observed at surface in this area represent melts derived from thick sequences of deeply buried pelitic sediments which were deposited in a continental margin ocean basin prior to collision of the Rae and Slave cratons. Concentration of graphite within the garnet-rich restite produced during melting could be the source of major conductors such as the deep crustal zone in the central portion of our model (Fig. 8A) that is spatially correlated with the main leucogranite belt. An obvious problem with this mechanism is the difference between the along-strike continuity of the leucogranite belt (Fig. 1) and the more complicated spatial pattern observed in the MT model (Fig. 9). Further work exploring the inter-line resolution of the MT model and spatial relationships to aeromagnetic features is of key importance. It should also be noted that images of the isostatic gravity anomaly (not shown here) representative of deep crustal density variations do not spatially correlate with the aeromagnetically defined distribution of leucogranites, as might be expected from the garnet-rich crust from which leucogranite was extracted. This may reflect the presence of garnet enriched restite formed during production of older, ca. 2.0 Ga plutonic belts, which have a geochemical signature pointing to garnet in their source region (Berman et al., 2015a). A more complicated structure may also reflect younger post-collisional readjustments associated with Slave-Rae docking, with post-collisional uplift breaking the interconnectedness of the films (Frost et al., 1989).

Alternatively, the complicated spatial morphology of the MT model may be ascribed to graphite films on grain boundaries arising from deep-seated granulite metamorphism which was widespread during the ca. 2.35 Ga Arrowsmith orogeny that affected Queen Maud block and Duggan Lake domain (Berman et al., 2015b). Granulite-facies conditions were also achieved during the ca. 2.0-1.9 Ga Thelon orogeny within the northern map sheet (76I), but have not been recognized to a similar extent in the southern map sheet (76H).

Although the mechanism of creating MT conductors remains to be established, the observed conductivity variations in the 3D model impact on the major tectonic question regarding the pedigree of basement underlying the western and central plutonic belts, i.e. the crustal block between recognized Slave and Rae cratons (Fig. 2). The Slave-Rae collisional model requires that this crust is Rae craton with ca. 2.0 Ga plutonic rocks representing a continental arc produced above an east-dipping subduction zone. This model would require revision if Slave crust underlies this region. The MT model results show that Mesoarchean crust of the Queen Maud block and Duggan Lake domains are underlain by highly conductive regions below ~10 km, whereas the conductivity anomalies below the Slave craton have much lower amplitude. In comparison, the strong conductor observed below the west and central

plutonic belts is very similar to those underlying Mesoarchean crust further east. This would suggest that this region is underlain by Mesoarchean crust of the Rae craton if the conductive crust formed prior to the Thelon orogeny, perhaps instead during the ca. 2.35 Ga Arrowsmith orogeny. A pre-Thelon orogeny origin is consistent with the disruption of the eastern conductors by a resistive column that aligns with the ca. 2.0 Ga eastern plutonic belt. However, we cannot rule out the possibility that the conductors formed in different crustal blocks that were affected by similar processes during the Thelon orogeny. At the present time this possibility seems less likely given the strong similarity of these conductive regions.

When comparing the 3D model west of site 204 (Fig. 8A) and west of site 105 (Fig. 8B), there is a variation in the appearance of the model that is poorly understood at present, but may be clarified by ongoing studies aimed at understanding the geological differences between these regions. The features in the model underlie in a broad sense rocks at the surface associated with granulite metamorphism. It is not unlikely perhaps that graphitized carbon films arising from granulite metamorphism would have a complicated morphology as the orthopyroxene-bearing gneisses in this area are highly deformed, presumably during the collision of the Slave and Rae and post-collisional indentation and strike slip faulting (Culshaw et al., 1991; Hoffman and Hall, 1993).

The conductor at the surface in the Slave craton links with a granitoid unit in the northern section (Fig. 8b), whereas the thin conductor in the southern section (Fig. 8a) underlies supracrustal rocks. These along strike variations are presently not understood. Finally, a shallow conductive feature appears near sites 203 and 204 in the centre of the profile and in both the 2-d and 3-d model. This feature is also observed in the northern section, but is less conductive. We tentatively ascribe it to graphite within the ca. 1.95 Ga metasedimentary package, but it could also reflect fluids or sulphides within a shallow fault structure.

Conclusions

High quality MT data were collected in support of the GEM-2 Thelon tectonic zone project. After processing and editing, a decomposition analysis was performed along the southern profile that resulted in estimates of the geo-electric strike of -19 degrees for the upper/mid crust and -47 degrees for lower crust and mantle. These two strike directions were used to produce a hybrid 2D model. This model is highlighted by two conductive zones that extend to 60-70 km depth along the profile and some discreet conductive areas at depths of 5-10 km near the centre of the line. 3D inversion of the data followed, using all of the MT sites except for one, and an acceptable preliminary model was achieved that can help start constraining the geological interpretations and be the basis for more fine-tuned inversion studies. The 2D and 3D models have some features that correlate, but also display some differences, which is understandable given the variations in the inversion techniques. The 3D inversion is able to restore out of plane features which the 2D model cannot, however, the 2D modelling is done with smaller cell sizes and, thus, enabling finer structure than 3D. With small exceptions the 3D model shows a uniformly resistive upper crust (1-10 km) and a very complex, more conductive mid/lower crust and upper mantle. Generally, the lower crust appears to be more resistive below the region associated with the Slave craton.

Acknowledgements

We would like to thank Bobby Klengenberg for his hard work in both keeping a watchful eye for wildlife and helping with the MT field site installs. Leo Nadeau and Joe Whalen also assisted at some of the MT site installs. Great Slave Helicopters provided wonderful support and helped maximize the amount of data that was collected.

References

Berman, R.G., Percival, J.A., Harris, J.R., Davis, W.J., McCurdy, M., Normandeau, P., Case, G., Nadeau, L., Hillary, E.M., Girard, E., Jefferson, C.W., Kellett, D., Camacho, A., Bethune, K., Pehrsson, S., and Bethune, K., 2015a. Geo-Mapping Frontiers' Chantrey project: bedrock geology and multidisciplinary supporting data of a 550 kilometre transect across the Thelon tectonic zone, Queen Maud block, and adjacent Rae craton; Geological Survey of Canada, Open File 7698.

Berman, R.G., Nadeau, L., Davis, W.J., McCurdy, M., Craven, J., McMartin, I., Whalen, J., Sanborn-Barrie, M., Carr, S., Pehrsson, S., Percival, J.A., and Girard, E., 2015b. New insights into the geological evolution and economic potential of the Thelon tectonic zone and western Rae craton, Nunavut; Geological Survey of Canada, Open File 7901, 1 sheet.

Booker, J.R., Burd, A., and Mackie, R., 2014, Three-dimensional magnetotelluric inversions can image structure outside an array: 22nd EM Induction Workshop Weimar, Germany, August 24-30, 2014

Chacko, T., De, S.K., Creaser, R.A., and Muehlenbachs, K., 2000. Tectonic setting of the Taltson magmatic zone at 1.9-2.0 Ga: A granitoid-based perspective; Canadian Journal of Earth Sciences, v. 37, p. 1597-1609.

Culshaw, N., 1991. Post-collisional oblique convergence along the Thelon tectonic zone, north of the Bathurst Fault, NWT, Canada; Journal of Structural Geology, v. 13, p. 501-516.

Davis, W., Berman, R.G., and MacKinnon, A., 2013. U-Pb Geochronology of Archival Rock Samples from the Queen Maud Block, Thelon Tectonic Zone and Rae Province, Kitikmeot Region, Nunavut, Canada; Geological Survey of Canada, Open File, v. 7409, p. 42p.

Davis, W.J., Berman, R.G., Nadeau, L., and Percival, J.A., 2014. U-Pb zircon geochronology of a transect across the Thelon tectonic zone, Queen Maud region, and adjacent Rae craton, Kitikmeot Region, Nunavut, Canada; Geological Survey of Canada, Open File 7652, 41p.

Frith, R.A., 1982. Geology, Beechey Lake-Duggan Lake, District of Mackenzie; Geological Survey of Canada, Open File, v. 851 (1:125,000).

Groom, R.W., and R.C. Bailey, 1989. Decomposition of magnetotelluric impedance tensors in the presence of local three-dimensional galvanic distortion; Journal of Geophysical Research, v. 94, p. 1913 – 1935.

Hoffman, P.F., 1988. United plates of America, the birth of a craton: Early Proterozoic assembly and growth of Laurentia; Annual Reviews of Earth and Planetary Science, v. 16, p. 543– 603.

Kerr, D.E., 1994. Late Quaternary stratigraphy and depositional history of the Parry Peninsula-Perry River area, District of Mackenzie, Northwest Territories; Geological Survey of Canada, Bulletin 465, 34 p.

Harris, N.B.W. and Inger, S., 1992, Trace element modelling of pelitic-derived granites, Contributuons to Mineralogy and Petrology, v.110, p.46-56.

Hoffman, P.F., and Hall, L., 1993. Geology, Slave Craton and environs, District of Mackenzie, Northwest Territories; Geological Survey of Canada, Open File, v. 2559, p. 1 sheet.

Jones, A.G., Chave, A.D., Egbert, G.D., Auld, D., and Barh, K., 1989. A comparison of techniques for magnetotelluric response function estimation; Journal of Geophysical Research, v. 94, 14210 – 14213.

Kiyan, D., Jones, A.G, and Vozar, J., 2014. The inability of magnetotelluric off-diagonal impedance tensor elements to sense oblique conductors in three-dimensional inversion, Geophysical Journal International, v.196, p.1351-1364.

Korja, T., Tuisku, P., Pernu, T. and Karhu, J. (1996), Field, petrophysical and carbon isotope studies on the Lapland Granulite Belt: implications for deep continental crust. Terra Nova, 8: 48–58.

McCurdy, M.W., Berman, R.G., Kerr, D.E., and Vaive, J.E., 2013. Geochemical, Mineralogical and Kimberlite Indicator Mineral Data for Silts, Heavy Mineral Concentrates and Waters, Duggan Lake Area, Nunavut (NTS 76H and 76I South); Geological Survey of Canada, Open File 7471.

McNeice, G.W., and A.G. Jones, 2001. Multisite, multifrequency tensor decomposition of magnetotelluric data; Geophysics, v. 66, p. 158 – 173.

Nabelek, P.I. and Liu, M., 2004, Petrologic and thermal constraints on the origin of leucogranites in collional orogens, Transactions of the Royal Society of Edinburgh: Earth Sciences, v. 95, p.73-85.

Rodi, W., and R.L. Mackie, 2001. Nonlinear conjugate gradients algorithm for 2-D magnetotelluric inversion, Geophysics, v. 66, p. 174 - 186.

Schultz, M.E.J., Chacko, T., Heaman, L.M., Sandeman, H.A., Simonetti, A., and Creaser, R.A., 2007. Queen Maud block: A newly recognized Paleoproterozoic (2.4-2.5 Ga) terrane in northwest Laurentia; Geology, v. 35, p. 707-710.

Thompson, P., 1986. Geology, Tinney Hills-Overby Lake (West Half), District of Mackenzie, Northwest Territories; Geological Survey of Canada, Open File, v. 1316 (1:125,000).

Thompson, P.H., Culshaw, N., Buchanan, J.R., and Manojlovic, P., 1986. Geology of the Slave Province and Thelon tectonic zone in the Tinney Hills-Overby Lake (west half) map area, District of Mackenzie; Geological Survey of Canada Paper, v. 86-1A, p. 275-289.

Thompson, P.H., 1989. An empirical model for metamorphic evolution of the Archaean Slave Province and adjacent Thelon tectonic zone, north-western Canadian Shield; *in* (eds) Daly, J.S., Cliff, R.A., and Yardley, B.W.D. Evolution of metamorphic belts, Geological Society Special Publication, v. 43, p. 245-263.

Table 2. Summary of MT acquisition

INSTALL Date	MT Site Name	Latitude	Longitude	Coils	MTU	Recording time (nights)	Notes
25-Jun-14	ttz100	65.8484	-105.3163	Hx:MT80H7320, Hy:MT80H7513, Hz:AMTC1328	1562	1	site near camp
26-Jun-14	ttz100			Hx:MT80H7320, Hy:MT80H7513, Hz:AMTC1328	1562	1	re-sound
27-Jun-14	ttz100			Hx:MT80H7320, Hy:MT80H7513, Hz:AMTC1328	1562	1	re-sound
28-Jun-14	ttz100			Hx:MT80H7320, Hy:MT80H7513, Hz:AMTC1328	1561	1	re-sound
29-Jun-14	ttz100			Hx:MT80H7320, Hy:MT80H7513, Hz:AMTC1328	1561	1	re-sound
26-Jun-14	ttz101	66.1929	-106.4992	Hx:MT80H7322, Hy:MT80H7509, Hz:AMTC1147	1493		failed
27-Jun-14	ttz101			Hx:MT80H7322, Hy:MT80H7509, Hz:AMTC1147	1493	1	re-sound
26-Jun-14	ttz102	66.2226	-105.7025	Hx:MT80H7319, Hy:MT80H8051	1496		failed
27-Jun-14	ttz102			Hx:MT80H7319, Hy:MT80H8051	1496		failed, moved to ttz102b
27-Jun-14	ttz102b			Hx:MT80H8051, Hy:MT80H7319, Hz:AMTC1145	1561		failed
09-Jul-14	ttz102			Hx:MT80C8053, Hy:MT80C8052, Hz:AMTC1145	1562		failed, battery problem
26-Jun-14	ttz103	66.2184	-105.3376	Hx:MT80C8053, Hy:MT80C8052	1561	1	
28-Jun-14	ttz104	66.1914	-105.1364	Hx:MT80H7319, Hy:MT80H8051	1561		failed
28-Jun-14	ttz104			Hx:MT80H7319, Hy:MT80H8051	1561		failed
30-Jun-14	ttz104			E-only	1561	1	
28-Jun-14	ttz105	66.1773	-104.8629	Hx:MT80H7322, Hy:MT80H7509	1493	1	
29-Jun-14	ttz106	66.1675	-104.5438	Hx:MT80H7509, Hy:MT80H7322, Hz:AMTC1147	1493	1	
29-Jun-14	ttz107	66.1491	-104.3037	Hx:MT80C8052, Hy:MT80C8053, Hz:AMTC1145	1562	1	
30-Jun-14	ttz108	66.1395	-103.8171	Hx:MT80C8052, Hy:MT80C8053, Hz:AMTC1145	1562		failed
01-Jul-14	ttz108			Hx:MT80C8052, Hy:MT80C8053, Hz:AMTC1145	1562	1	re-sound, 2 batts
03-Jul-14	ttz201	65.632	-106.5888	Hx:MT80C8052, Hy:MT80C8053, Hz:AMTC1145	1562	4	prog for 4 days
02-Jul-14	ttz202	65.6905	-105.7237	Hx:MT80H7509, Hy:MT80H7322, Hz:AMTC1147	1493	1	
30-Jun-14	ttz203	65.6896	-105.3268	Hx:MT80H7509, Hy:MT80H7322, Hz:AMTC1147	1493	1	
01-Jul-14	ttz203			Hx:MT80H7509, Hy:MT80H7322, Hz:AMTC1147	1493		re-sound - failed
01-Jul-14	ttz204	65.7127	-105.1276	Hx:MT80H7320, Hy:MT80H7513, Hz:AMTC1328	1496	(7 hrs)	failed
02-Jul-14	ttz204			Hx:MT80H7320, Hy:MT80H7513, Hz:AMTC1328	1496		failed
03-Jul-14	ttz204			Hx:MT80H7320, Hy:MT80H7513, Hz:AMTC1328	1496	1	re-sound
03-Jul-14	ttz205	65.6976	-104.9096	Hx:MT80H7509, Hy:MT80H7322, Hz:AMTC1147	1493	1	
04-Jul-14	ttz206	65.6985	-104.598	Hx:MT80H7509, Hy:MT80H7322, Hz:AMTC1147	1493	1	
05-Jul-14	ttz206			Hx:MT80H7509, Hy:MT80H7322, Hz:AMTC1147	1493	1	re-sound
04-Jul-14	ttz207	65.7081	-104.3661	Hx:MT80H7513, Hy:MT80H7320, Hz:AMTC1328	1496	1	
05-Jul-14	ttz207			Hx:MT80H7513, Hy:MT80H7320, Hz:AMTC1328	1496	1	re-sound
06-Jul-14	ttz208	65.7205	-104.0551	Hx:MT80H7509, Hy:MT80H7322, Hz:AMTC1147	1493	1	
08-Jul-14	ttz208			Hx:MT80H7509, Hy:MT80H7322, Hz:AMTC1147	1561	1	re-sound
06-Jul-14	ttz209	65.7032	-103.6628	Hx:MT80H7320, Hy:MT80H7513, Hz:AMTC1328	1496	1	
07-Jul-14	ttz210	65.6848	-105.9555	Hx:MT80C8053, Hy:MT80C8052	1562	2	prog for 2 days
08-Jul-14	ttz211	65.8508	-105.0144	Hx:MT80H7320, Hy:MT80H7513, Hz:AMTC1328	1496	1	
10-Jul-14	ttz212	65.8607	-104.762	Hx:MT80H7509, Hy:MT80H7322, Hz:AMTC1147	1561	1	
12-Jul-14	ttz213	65.8462	-105.5428	Hx:MT80C8053, Hy:MT80C8052, Hz:AMTC1145	1562	1	

Appendix A. Response curves (resistivity and phase) after processing and editing for all TTZ MT sites.

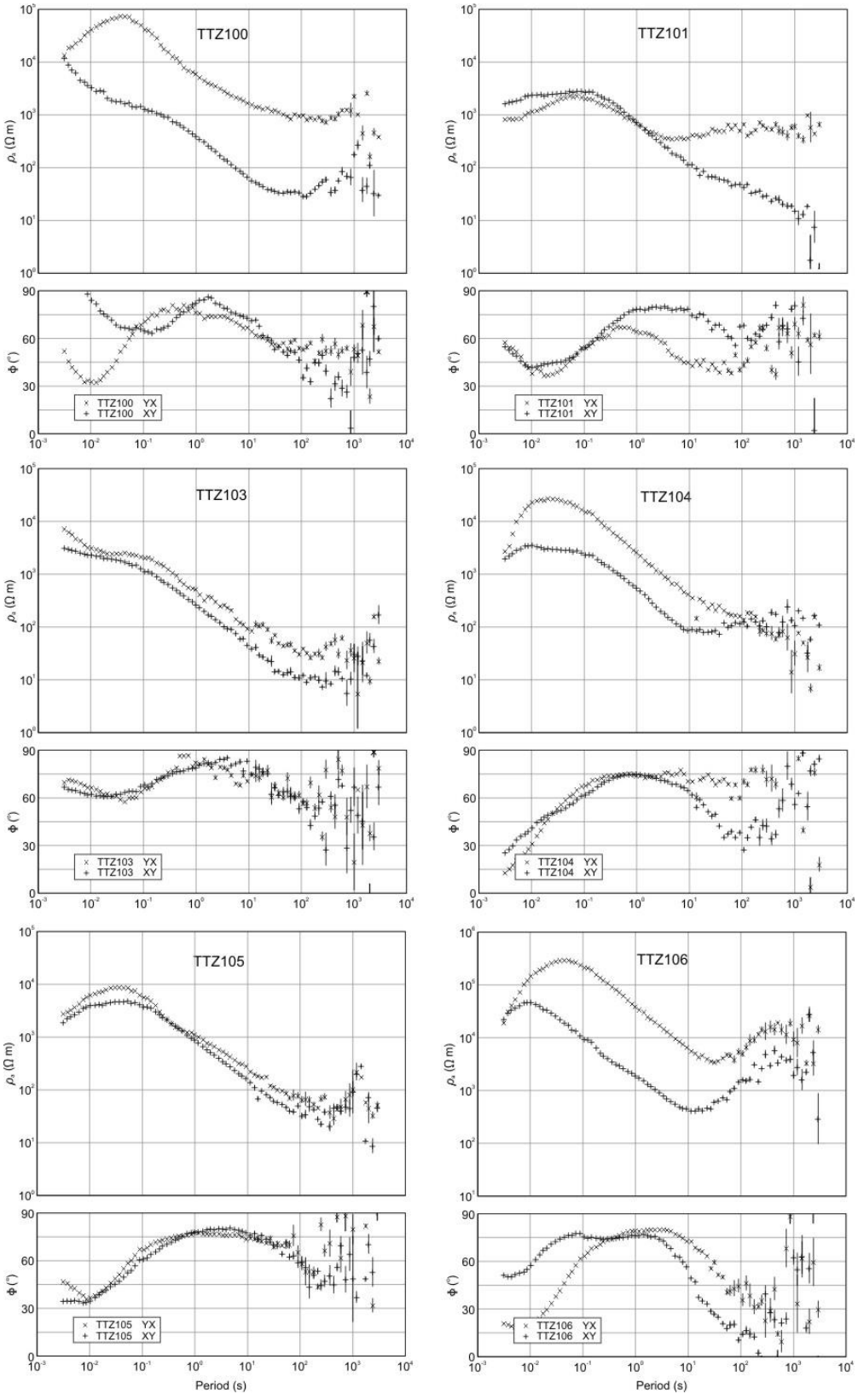

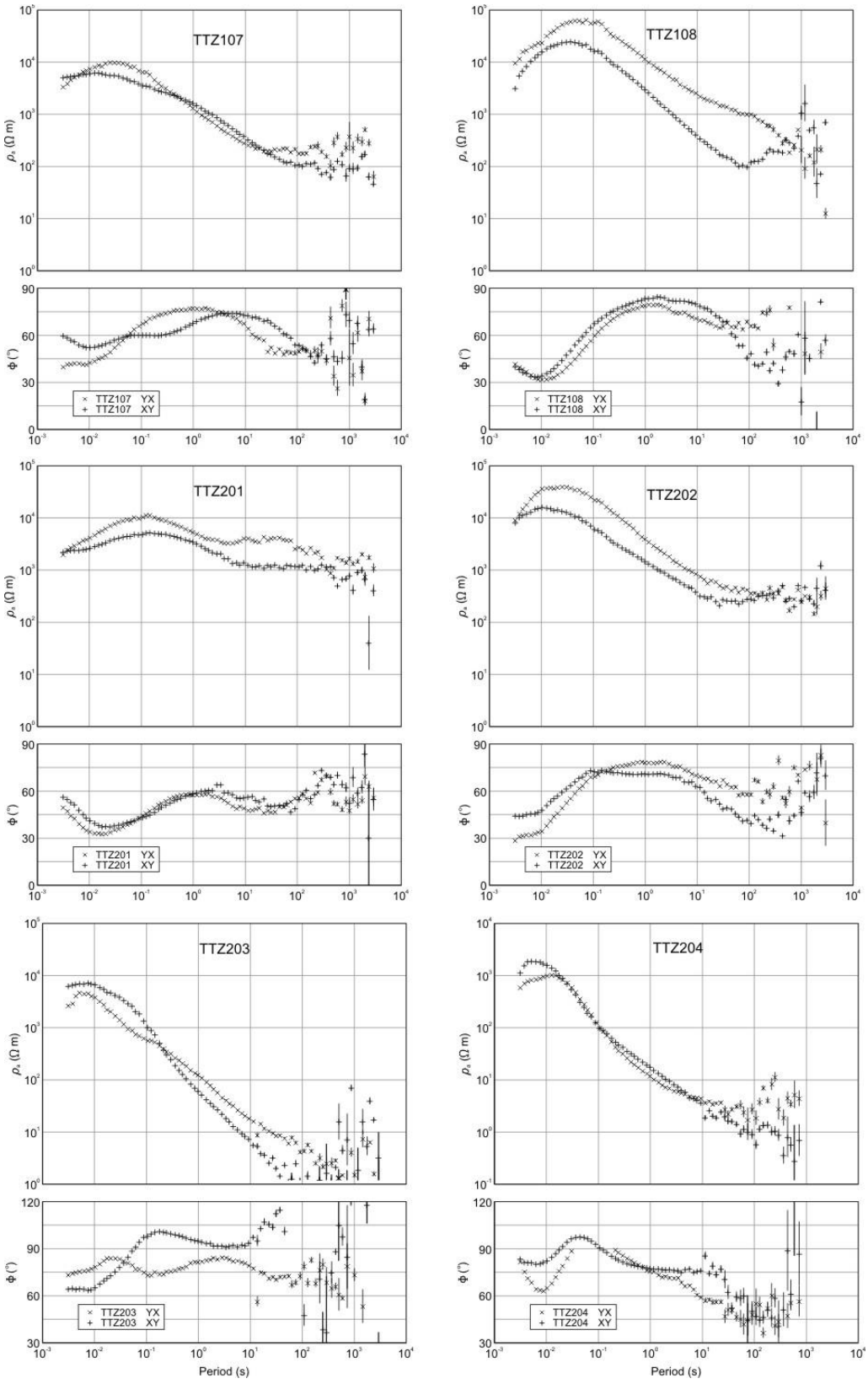
TTZ107
TTZ108
TTZ201
TTZ202
TTZ203
TTZ204
ρ_a (Ω m)
Φ (°)
TTZ107 YX
TTZ107 XY
TTZ108 YX
TTZ108 XY
TTZ201 YX
TTZ201 XY
TTZ202 YX
TTZ202 XY
TTZ203 YX
TTZ203 XY
TTZ204 YX
TTZ204 XY
Period (s)

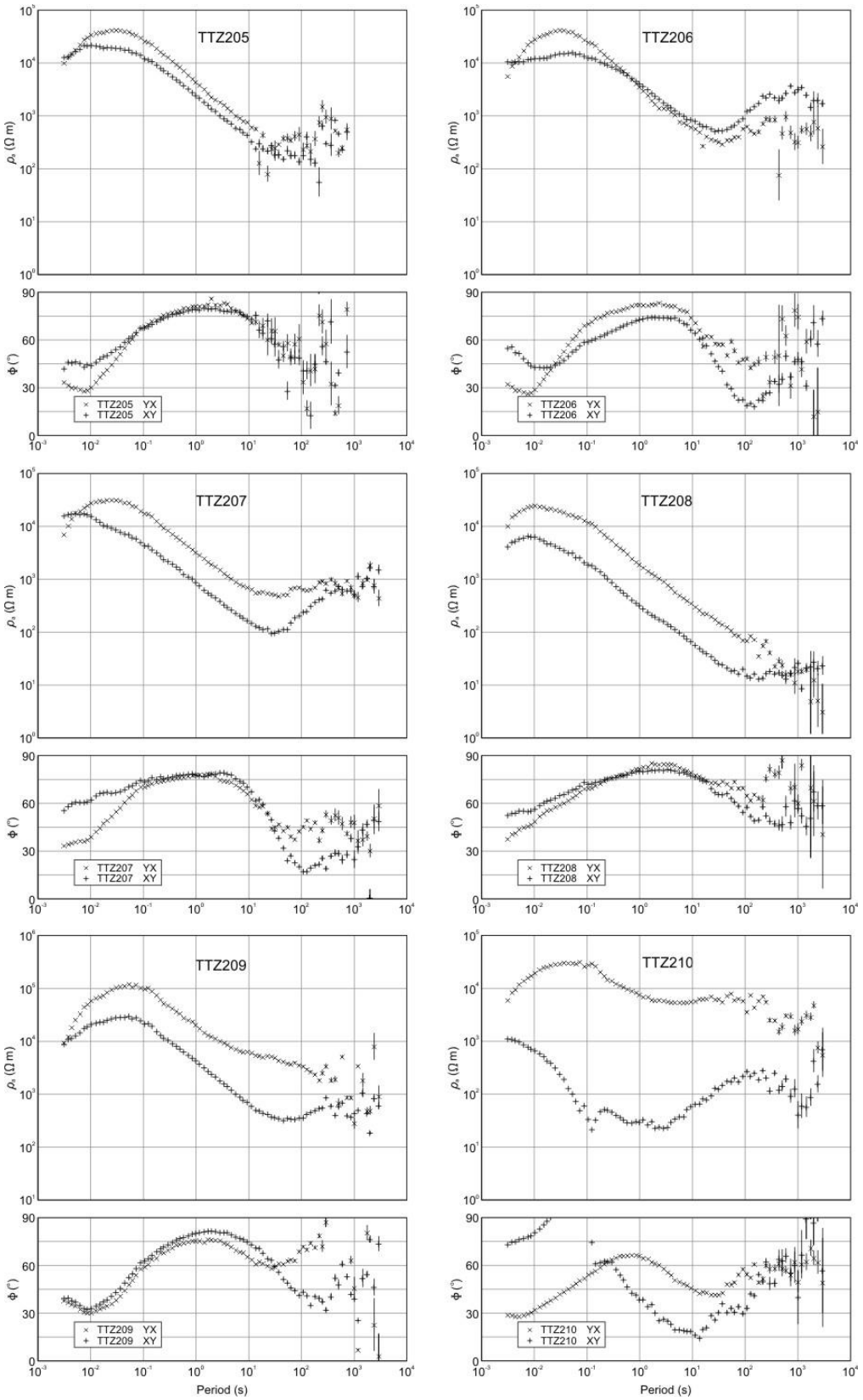
TTZ205
TTZ206
TTZ207
TTZ208
TTZ209
TTZ210
ρa (Ω m)
Φ (°)
TTZ205 YX
TTZ205 XY
TTZ206 YX
TTZ206 XY
TTZ207 YX
TTZ207 XY
TTZ208 YX
TTZ208 XY
TTZ209 YX
TTZ209 XY
TTZ210 YX
TTZ210 XY
Period (s)

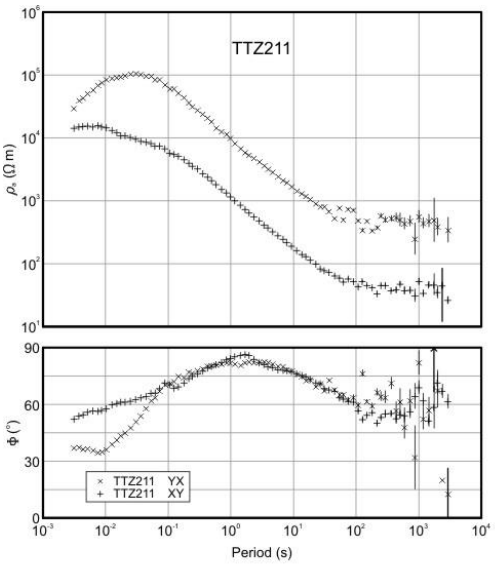
TTZ211
ρ_a (Ω m)
Φ (°)
TTZ211 YX
TTZ211 XY
Period (s)

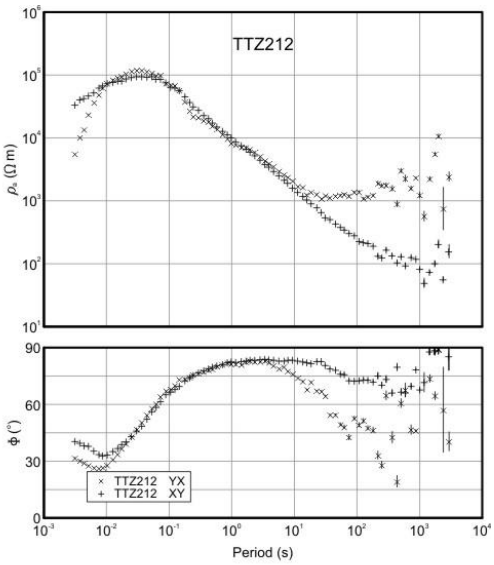
TTZ212
ρ_a (Ω m)
Φ (°)
TTZ212 YX
TTZ212 XY
Period (s)

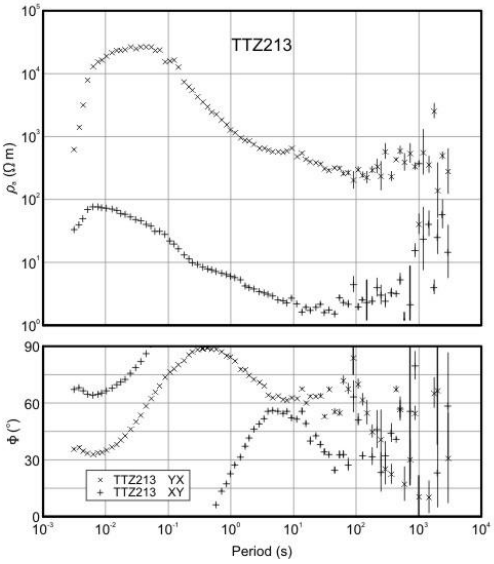
TTZ213
ρ_a (Ω m)
Φ (°)
TTZ213 YX
TTZ213 XY
Period (s)

Appendix B. Response curves (Azimuth = -19 degrees) for TTZ MT sites (black circles XY component, white circle YX component) and corresponding match from the 3D model presented in this report (solid lines).

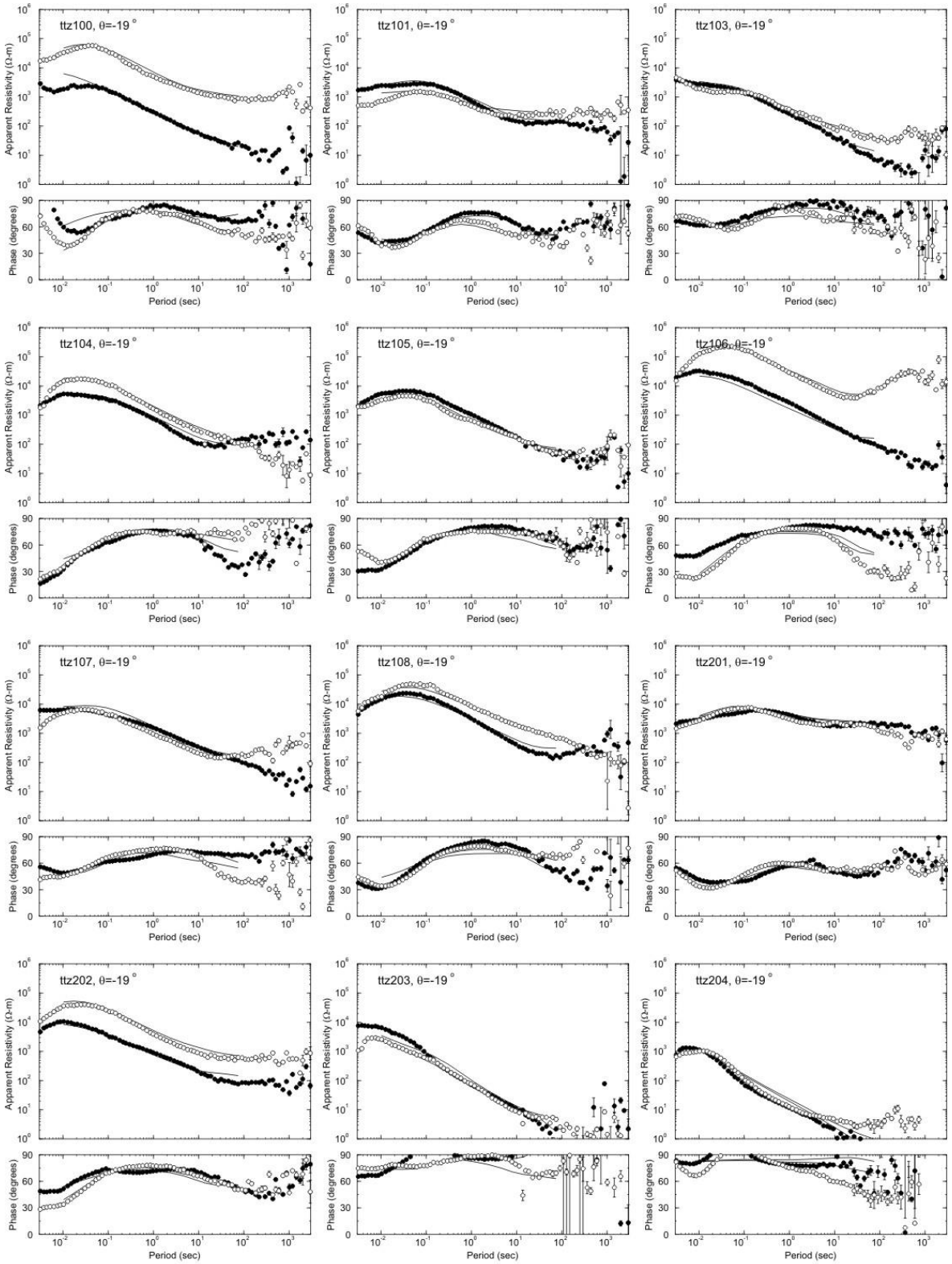

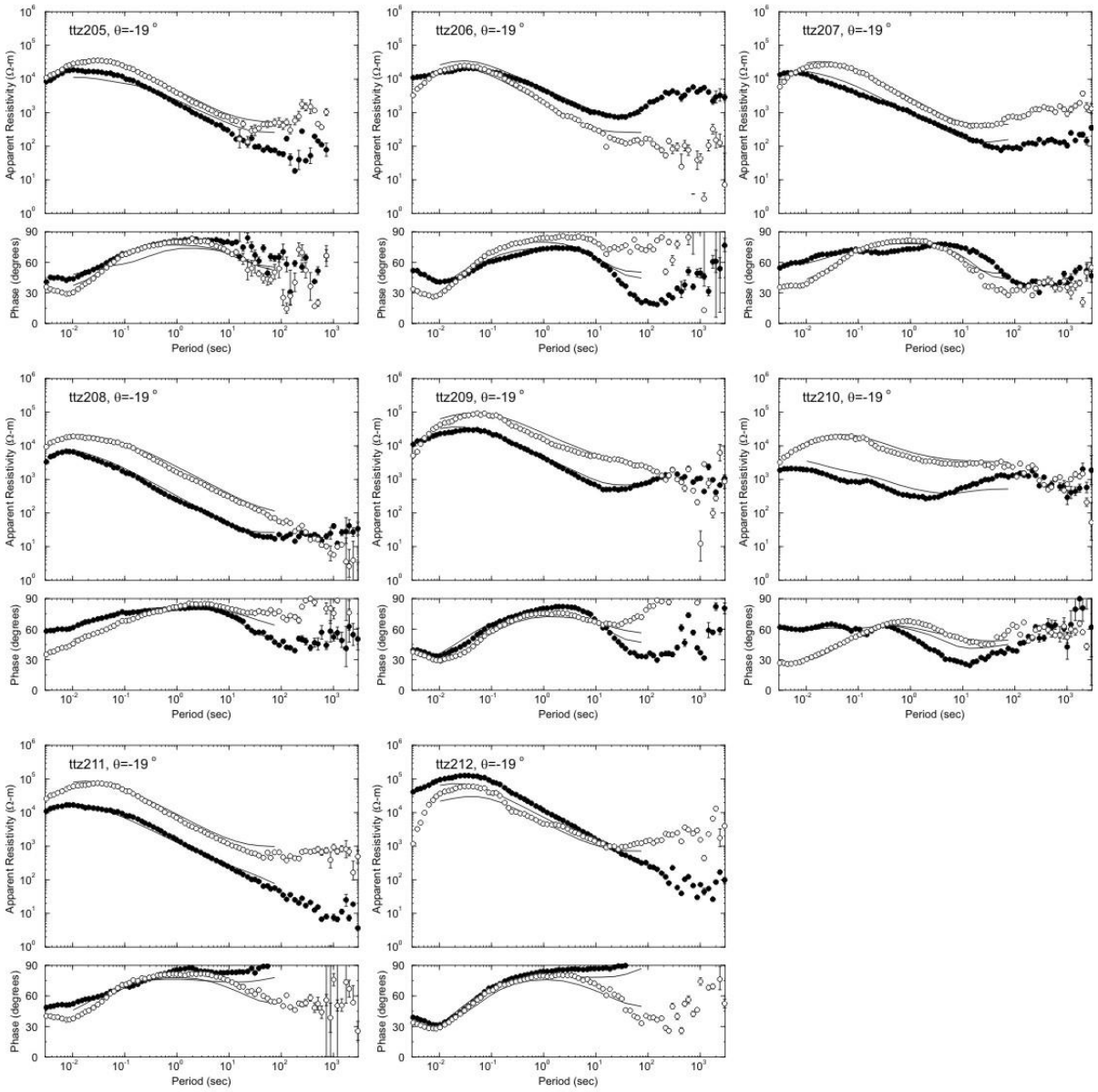

model3a Iter: 2 RMS: 1.7806 : Plotted Mar 19 2015 @ 11:45